Available online at www.sciencedirect.com

SciVerse ScienceDirect

Scripta Materialia 68 (2013) 639–642

Scripta MATERIALIA

www.elsevier.com/locate/scriptamat

Deformation crossover in nanocrystalline Zr micropillars: The strongest external size

J.Y. Zhang, J.C. Cui, G. Liu* and J. Sun*

State Key Laboratory for Mechanical Behavior of Materials, Xi'an Jiaotong University, Xi'an 710049, People's Republic of China

Received 28 November 2012; revised 18 December 2012; accepted 19 December 2012
Available online 2 January 2013

For small-scale metallic single crystals, systematic studies have established that external sample size (ϕ) has an obvious influence on the apparent strength, following a "smaller is stronger" fashion. In the present nanocrystalline (NC) Zr micropillars, deformation crossover leads to the strongest external size emerging at a critical $\phi \approx 400$ nm, similar to that of bulk-scaled NC metals. Above the critical external size the NC Zr pillars failed via highly inhomogeneous single-shear offset, below which they deformed via relative homogeneous shear.

Keywords: Nanocrystalline Zr micropillar; Plastic deformation; Strength; Size effect

According to conventional solid mechanics, the strength of a bulk scale metal only depends on its internal structure or feature size, which in turn is controlled by the processing steps chosen for its fabrication [1,2]. However, this view is based on being able to select a representative volume element (RVE) of the solid that incorporates all of the microstructural characteristics of a correspondingly larger volume element, since the plastic properties of a metal are governed by the characteristic length scale of a particular microstructure, thereby dictating the bulk material's strength as a function of, for example, grain or precipitate size, twin or layer thickness, or dislocation density [2–4]. Once the external sample size is significantly greater than the largest of these length scales, one observes sample-size-independent plastic behavior. In conventional bulk polycrystalline metals, grain boundaries (GBs) obscure the passage of the gliding dislocations, providing effective barriers to transmission of dislocations from one grain to the next, rendering the strength dependent on grain size via the well-known Hall–Petch mechanism [4,5]. When the grain size (d) falls below a critical value (at the nanoscale ~15–20 nm), the role of the GBs shifts toward dislocation and absorption sites and sometimes to the deformation path itself [4,6,7], which renders the inverse size effect, i.e. the so-called "inverse Hall–Petch relation" in nanocrystalline (NC) metals [8,9]. The deformation crossover from dislocation-mediated mechanism to GB-mediated mechanism leads to the strongest grain size [10,11].

However, in the past decade, the vast majority of uniaxial deformation experiments on small-scale metallic structures have unambiguously demonstrated that at the micron and sub-micron scales, the view that external size-independent plastic deformation occurs in bulk scale metals no longer holds true. In fact, it has been shown that the strength of single crystals scales with their external size in a power-law fashion, even approaching a significant fraction of the material's ideal strength, and exhibiting the well-known phenomenon "smaller is stronger" [1–4,6,12–14]. While significant effort has been dedicated to studying the mechanical behavior of single crystals at small scales, the effect of internal interfaces contained within nanometer-sized samples on strength and plastic deformation has not been studied to the same extent. Since both the internal (i.e. microstructure) characteristic size and external sample dimension (i.e. sample size) play a non-trivial role in the mechanical properties and material deformation mechanisms, it is critical to develop an understanding of their interplay and mutual effects on the mechanical properties and material deformation, especially in small-scale structures.

In this work, we investigated the compressive plastic flow of NC Zr micropillars with internal grain size (d) $\sim 35 \pm 15$ nm and external sample size (ϕ) spanning from 250 to 1200 nm by using microcompression

* Corresponding authors. Tel.: +86 (0) 2982668695; fax: +86 (0) 2982663453; e-mail addresses: lgsammer@mail.xjtu.edu.cn; junsun@mail.xjtu.edu.cn

1359-6462/$ - see front matter © 2012 Acta Materialia Inc. Published by Elsevier Ltd. All rights reserved.
http://dx.doi.org/10.1016/j.scriptamat.2012.12.024

methodology. It is revealed that the strongest external sample size emerges at ~400 nm, at which the NC Zr pillars exhibit uniform barreling. Above the critical size the NC Zr pillars exhibit localized major single shear offset; below this size the Zr pillars exhibit relatively homogeneous deformation.

Silicon-supported ~1.2 μm thick Zr thin film was synthesized by means of direct current magnetron sputtering at room temperature. The X-ray diffraction pattern of the as-deposited NC Zr thin films revealed ⟨10-10⟩, ⟨0002⟩ and ⟨10-11⟩ peaks, indicative of random orientations. The focused ion beam (FIB) machined micropillars, with ϕ spanning from 250 to 1200 nm, fabricated from the NC Zr thin, films were then uniaxially compressed in a Hystron Ti 950 triboindenter with a 10 μm side flat quadrilateral cross-section diamond indenter at a constant strain rate of $2 \times 10^{-4}\ s^{-1}$ up to 15–30% strain. More details on the fabrication procedure of the NC Zr micropillars can be found elsewhere [15,16]. Force–displacement data were continuously recorded, and the initial geometry of the micropillar was measured from scanning electron microscopy (SEM) images (see Fig. 1). The cross-sectional area at half height of the pillar (A_0) and the initial height (L_0) were used for calculations. Following our previous works [15,16]. True stress–strain curves were used to characterize the deformation behaviors. After consideration of the substrate effect and correcting for taper, the true strain ε_T and true stress σ_T are simply expressed as [17]:

$$\varepsilon_T = \frac{1+\frac{L_0}{r_0}\tan\psi}{E_{measured}}\frac{PL_p}{A_0L_0} + \ln\left(\frac{L_0}{L_p}\right), \quad (1)$$

and

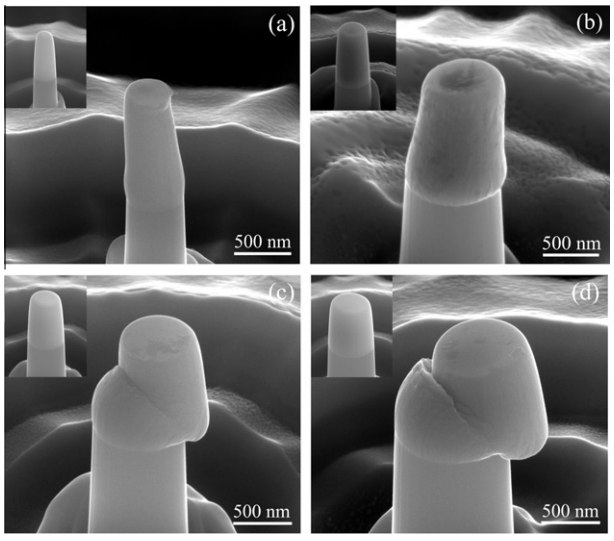

Figure 1. Typical FIB/SEM images of NC Zr micropillars with four different diameters (ϕ) after the uniaxial compression tests. (a) $\phi = 250$ nm micropillars show relatively homogeneous shear at the upper part of the micropillar; (b) $\phi = 420$ nm micropillars show uniform barreling of at strain ~15%; (c) $\phi = 600$ nm and (d) $\phi = 800$ nm micropillars showing a single shear offset of the NC Zr micropillars. Inset is the corresponding FIB/SEM images of the as-milled NC Zr micropillar.

$$\sigma_T = \frac{P}{A_p} = \frac{P}{A_0L_0}\left\{L_0 - \left[u_{tot} - \frac{\sqrt{\pi}P(1-\nu_{Zr}^2)}{2E_{Si}\sqrt{A_{Si}}}\right]\right\}, \quad (2)$$

where A_0 is the cross-sectional area at half the initial height (L_0) of the pillar; r_0 is the radius at the top of the pillar; L_p and A_p are the final height and average cross-sectional area, respectively; P is the load; E_{Zr} is the true modulus of Zr pillars without tapers and $E_{measured}$ is the measured modulus of the tapered Zr pillars; u_{tot} is the total displacement; ν_{Zr} is the Poisson's ratio of Zr (~0.3); A_{Si} and E_{Si} are respectively the average cross-sectional area and the modulus of the substrate Si pillar. Note that the influence of taper (ψ) has been taken into account in the above equations [17].

Figure 1a–d and their insets present FIB/SEM micrographs of the NC Zr micropillars before and after the test. It is clearly revealed that when the external size ϕ is smaller than ~400 nm, the NC Zr micropillars exhibited relatively homogeneous deformation (pillar sheared at the rounded top part [18,19]), at which the Zr micropillars uniformly deformed (barreling) at plastic strain <15%. Above the critical external size ~400 nm, the NC Zr micropillars failed via localized inhomogeneous shear deformation (the pillar sheared with a major shear offset, i.e. a single shear offset is observed to initiate at the side surface and run across the entire pillar). In other words, there is an apparent transition in shearing mode from highly inhomogeneous shear to relatively homogeneous shear as the external size decreases. This transition of deformation modes caused by the external size limitation has been observed in amorphous micropillars [18–20], nanolayered crystalline Cu/Zr [15,16] and crystalline/amorphous Cu/Cu–Zr [17,21,22] micropillars. These observations support the notion that reduction in external size may shift the deformation mode to that typical of much smaller internal sized and amorphous metallic systems, regardless of the underlying deformation mechanism. In fact, in submicron-sized NC pillars the presence of free surfaces activates these GB-mediated processes, such as GB sliding and grain rotation, at much larger grain sizes than observed in the bulk-scaled NC materials [23], as is consistent with the molecular dynamics (MD) simulations results in NC Pt nanopillars [24]. Under ultrahigh external mechanical stress, once a mesoscopic glide plane is formed, localized sliding shear can result in macroscopic sliding over the dimensions of many grains and eventually lead to a large strain based on the GB sliding mechanism [15,25], without significant oscillatory or intermittent burst of the stress–strain curve (see Fig. 2a). Such a mechanism also operates in nanolayered crystalline Cu/Zr micropillars [15,16], triggering shear failure. In contrast, the catastrophic shear failure associated with the burst in the stress–strain curve frequently occurred in glassy materials via the activation of shear transformation zones (STZs) [17,21,22,26]. However, due to the constraining effect of strong NC Cu layers on glassy Cu–Zr layers the catastrophic shear failure observed in monolithic amorphous materials can be suppressed in crystalline Cu/amorphous Cu–Zr micropillars/nanolaminates, which is supported by their smooth compressive/tensile stress–strain curves [17,21,22,26]. Specifically, Zhang et al. [17] recently revealed that shear deformation can

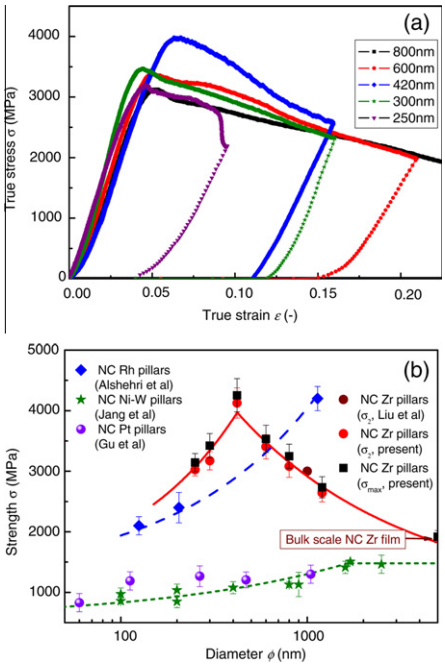

Figure 2. (a) True stress–strain plot for NC Zr micropillars with various ϕ. (b) The dependence of strength on pillar diameter. For comparison, results from other reports on the diameter ϕ-dependent strength of NC Zr [30], Ni–W [23], Pt [24] and Rh [28] micropillars are also included in this figure. The lines are visual guides.

still be observed in crystalline/amorphous Cu/Cu–Zr micropillars at smaller intrinsic layer thickness (<20 nm), which also exhibited the transition from inhomogeneous shear to relatively homogeneous shear with reducing extrinsic sample dimension. Although at such small thicknesses, <20 nm, the glassy layers can exhibit homogeneous deformability [21,22], the fracture of glassy layers under external stress (greater than their ideal strength) can cause shear failure of the whole crystalline/amorphous micropillars [17].

Figure 2a presents typical true stress–strain curves of four NC Zr pillars with $\phi = 300,\ 420,\ 600$ and 800 nm. It is found that these smooth true stress–strain curves are characterized by an initial segment of elastic loading (approaching high stress) and subsequent rapid stress drop (softening). This is similar to that of observed in $\phi = 140$ nm glassy Cu50Zr50 pillars [27]. Unlike the amorphous materials whose shear band formed via shear transformation zone (STZ)-mediated activities (STZ percolation/collection) [18–20], the major shear offset can form via GB-mediated processes such as GB sliding and grain rotation in NC metallic materials. At the same time, the operation of GB-mediated mechanisms, in general, cause softening behavior of metals, as is supported by the true stress–strain curves (see Fig. 2a).

Another striking feature is that as the deformation modes transit from inhomogeneous to homogeneous deformation, the strongest external size emerges at a critical size $\phi = 400$ nm with maximum strength (σ_{max}) ~4200 MPa, as shown in Figure 2b. Above the critical value the NC Zr pillars exhibit the "smaller is stronger" behaviour that can be described by a power law: $\sigma \propto \phi^{-0.48}$; below this critical value the inverse external size effect, i.e. "smaller is weaker", is observed. Similar results are observed in NC Ni–W [23], Pt [24] and Rh [28] micropillars as well as NC metals [4], regardless of the intrinsic properties (e.g. grain size, crystalline structure and stacking fault energy) of the materials, see Figure 2b. Such a external size effect only arises from the surface-related operation of dislocation sources [29], since the present NC Zr pillars should correspond to samples large with respect to an RVE without a suitable bulk source as discussed above. In such case, as ϕ is reduced, the likelihood that these smaller volumes contain any dislocation (source) is further reduced, which would result in sample-size-dependent plastic behavior. Recently, Jang and Greer [23] observed a transition in the deformation mechanism—from dislocation-driven deformation in $d \approx 60$ nm sized Ni–W pillars with diameters larger than 100 nm to GB-mediated deformation in pillars of 100 nm and below, previously observed only in grain sizes below 20 nm in materials of the same composition. They postulated that the presence of free surfaces activates these GB-mediated deformation processes, which appears to be facilitated by a reduction in external sample size [23]. Recent MD simulations [24] also indicated that interior of the nanopillars underwent plastic deformation via a mechanism involving dislocations that nucleated from GB triple junctions, then rapidly propagated across a grain and were absorbed by the opposite GB, similar to that of observed in bulk NC samples. Near the free surface, however, the deformation was found to be dominated by GB-mediated processes owing to the weak constraining interaction among grains, which results in the formation of small surface steps (i.e. small shear offsets) of the order of the atomic spacings at some of the GB/surface intersections [24].

In present work, the "smaller is stronger" trend excludes the possibility of GB-mediated softening or dislocation-driven softening caused by fewer GBs [28] being the dominant mechanism in smaller-sized NC Zr pillars at the initial stage. Instead, the GB dislocation sources provide the plastic carriers—dislocations to sustain the plastic flow. Specifically, Liu et al [30] observed the deformation twins in the deformed Zr layers (with thickness ~880nm and grain size d ~30 nm in amorphous Cu-Zr/crystalline Zr multilayered micropillars), further supporting the MD prediction that the (partial) dislocations nucleated from the GBs contribute to the plastic deformation. In addition, the mutual constraining effects of neighboring grains also hinder the GB-mediated processes that switch on at high stress levels. However, as the configurations of GBs are altered at greater stress (or strain), the GB-mediated processes is activated, triggering the softening behavior and shear deformation. This is consistent with the SEM observations that uniform barreling is observed at small strains, <15% (Fig. 1b), while a major shear offset occurs at large strains (Fig. 1c and d). In contrast, below the critical external size, the weaker constraining effects of neighboring grains render operation of the GB-mediated processes much easier in smaller-sized NC Zr pillars. As such, two competing processes may emerge simultaneously upon the introduction of internal interfaces into

smaller NC Zr pillars: dislocation-driven (or Hall–Petch-like) strengthening and GB-mediated weakening. The deformation crossover from mechanisms dominated by dislocation-mediated processes to GB-mediated processes induces the strongest external sample size in NC pillars, analogous to that of conventional NC metals.

In summary, there appears to be a crossover in the deformation mechanism that is facilitated by sample size reduction—from strengthening dominated by dislocations in NC Zr micropillars with diameters greater than ~400 nm to softening dominated by GBs in smaller micropillars, for which (~400 nm) the external size conferring the greatest strength is observed. Above the critical external size, the NC Zr pillar manifests itself in a "smaller is stronger" fashion failure via inhomogeneous single shear offset, while below the critical sample size the Zr pillars show the inverse external size effect ("smaller is weaker") accompanied by relatively homogeneous shear deformation.

This work was supported by the National Natural Science Foundation of China (Grant Nos. 50971097, 51201123), the 973 Program of China (Grant No. 2010CB631003), and the 111 Project of China (B06025). G.L. is grateful for support from the Fundamental Research Funds for the Central Universities and the Tengfei Scholar project. J.Y.Z. thanks the China Postdoctoral Science Foundation funded project for financial support (2012M521765).

[1] E. Arzt, Acta Mater. 46 (1998) 5611.
[2] J.R. Greer, J.T.M. De Hosson, Prog. Mater. Sci. 56 (2011) 654.
[3] E. Arzt, G. Dehm, P. Gumbsch, O. Kraft, D. Weiss, Prog. Mater. Sci. 46 (2001) 283.
[4] M.A. Meyers, A. Mishra, D.J. Benson, Prog. Mater. Sci. 51 (2006) 427.
[5] M. Dao, L. Lu, R.J. Asaro, J.T.M. De Hosson, E. Ma, Acta Mater. 55 (2007) 4041.
[6] T. Zhu, J. Li, Prog. Mater. Sci. 55 (2010) 710.
[7] D.C. Jang, C. Cai, J.R. Greer, Nano Lett. 11 (2011) 1743.
[8] C.E. Carlton, P.J. Ferreira, Acta Mater. 55 (2007) 3749.
[9] J. Schiotz, K.W. Jacobsen, Science 301 (2003) 1357.
[10] A.S. Argon, S. Yip, Philos. Mag. Lett. 86 (2006).
[11] V. Yamakov, D. Wolf, S.R. Phillpot, A.K. Mukherjee, H. Gleiter, Philos. Mag. Lett. 83 (2003) 385.
[12] G. Dehm, Prog. Mater. Sci. 54 (2009) 664.
[13] M.D. Uchic, P.A. Shade, D.M. Dimiduk, Annu. Rev. Mater. Res. 39 (2009) 361.
[14] O. Kraft, P.A. Gruber, R. Mönig, D. Weygand, Annu. Rev. Mater. Res. 40 (2010) 293.
[15] J.Y. Zhang, S.Y. Lei, Y. Liu, J.J. Niu, Y. Chen, G. Liu, X. Zhang, J. Sun, Acta Mater. 60 (2012) 1610.
[16] J.Y. Zhang, S. Lei, J. Niu, Y. Liu, G. Liu, X. Zhang, J. Sun, Acta Mater. 60 (2012) 4054.
[17] J.Y. Zhang, G. Liu, S.Y. Lei, J.J. Niu, J. Sun, Acta Mater. 60 (2012) 7183.
[18] C.Q. Chen, Y.T. Pei, J.T.M. De Hosson, Acta Mater. 58 (2010) 189.
[19] O.V. Kuzmin, Y.T. Pei, C.Q. Chen, J.T.M. De Hosson, Acta Mater. 60 (2012) 889.
[20] C.C. Wang, J. Ding, Y.Q. Cheng, J.C. Wan, L. Tian, J. Sun, Z.W. Shan, J. Li, E. Ma, Acta Mater. 60 (2012) 5370.
[21] J.Y. Kim, X. Gu, M. Wraith, J.T. Uhl, K.A. Dahmen, J.R. Greer, Adv. Funct. Mater. 22 (2012) 1972.
[22] J.Y. Kim, D.C. Jang, J.R. Greer, Adv. Funct. Mater. 21 (2011) 4550.
[23] D. Jang, J.R. Greer, Scripta Mater. 64 (2011) 77.
[24] X.W. Gu, C.N. Loynachan, Z. Wu, Y.W. Zhang, D.J. Srolovitz, J.R. Greer, Nano Lett. (2012), http://dx.doi.org/10.1021/nl3036993.
[25] Y. Ivanisenko, L. Kurmanaeva, J. Weissmueller, K. Yang, J. Markmann, H. Rösner, T. Scherer, H.J. Fecht, Acta Mater. 57 (2009) 3391.
[26] Y.M. Wang, J. Li, A.V. Hamza, J.T.W. Barbee, Prog. Natl. Acad. Sci. USA 104 (2007) 11155.
[27] M.C. Liu, J.C. Huang, K.W. Chen, J.F. Lin, W.D. Li, Y.F. Gao, T.G. Nieh, Scripta Mater. 66 (2012) 817.
[28] O. Alshehri, M. Yavuz, T. Tsui, Acta Mater. 61 (2012) 40.
[29] A. Rinaldi, P. Peralta, C. Friesen, K. Sieradzki, Acta Mater. 56 (2008) 511.
[30] M.C. Liu, J.C. Huang, H.S. Chou, Y.H. Lai, C.J. Lee, T.G. Nieh, Scripta Mater. 61 (2009) 840.